

Article

Demonstration of Thin Film Bulk Acoustic Resonator Based on AlN/AlScN Composite Film with a Feasible K_{eff}^2

Laixia Nian¹, Yang Zou¹, Chao Gao¹ , Yu Zhou¹, Yuchen Fan¹, Jian Wang¹, Wenjuan Liu¹ , Yan Liu¹ , Jeffrey Bowoon Soon², Yao Cai^{1,2,*}  and Chengliang Sun^{1,2,*} 

¹ The Institute of Technological Sciences, Wuhan University, Wuhan 430072, China

² School of Microelectronics, Wuhan University, Wuhan 430072, China

* Correspondence: caiyao999@whu.edu.cn (Y.C.); sunc@whu.edu.cn (C.S.)

Abstract: Film bulk acoustic resonators (FBARs) with a desired effective electromechanical coupling coefficient (K_{eff}^2) are essential for designing filter devices. Using AlN/AlScN composite film with the adjustable thickness ratio can be a feasible approach to obtain the required K_{eff}^2 . In this work, we research the resonant characteristics of FBARs based on AlN/AlScN composite films with different thickness ratios by finite element method and fabricate FBAR devices in a micro-electromechanical systems process. Benefiting from the large piezoelectric constants, with a 1 μm -thick Al_{0.8}Sc_{0.2}N film, K_{eff}^2 can be twice compared with that of FBAR based on pure AlN films. For the composite films with different thickness ratios, K_{eff}^2 can be adjusted in a relatively wide range. In this case, a filter with the specific N77 sub-band is demonstrated using AlN/Al_{0.8}Sc_{0.2}N composite film, which verifies the enormous potential for AlN/AlScN composite film in design filters.



Citation: Nian, L.; Zou, Y.; Gao, C.; Zhou, Y.; Fan, Y.; Wang, J.; Liu, W.; Liu, Y.; Soon, J.B.; Cai, Y.; et al.

Demonstration of Thin Film Bulk Acoustic Resonator Based on AlN/AlScN Composite Film with a Feasible K_{eff}^2 . *Micromachines* **2022**, *13*, 2044. <https://doi.org/10.3390/mi13122044>

Academic Editors: Junhui Hu and Ming Yang

Received: 30 September 2022

Accepted: 7 November 2022

Published: 22 November 2022

Publisher's Note: MDPI stays neutral with regard to jurisdictional claims in published maps and institutional affiliations.



Copyright: © 2022 by the authors. Licensee MDPI, Basel, Switzerland. This article is an open access article distributed under the terms and conditions of the Creative Commons Attribution (CC BY) license (<https://creativecommons.org/licenses/by/4.0/>).

Keywords: film bulk acoustic resonator; aluminum scandium nitride; composite film; effective electromechanical coupling coefficient

1. Introduction

For achieving a high-speed and large-capacity data exchange in the wireless communication, filters as key elements in the radio-frequency front-end module are desired to possess large bandwidth, high frequency, and low insertion [1–4]. Adopting aluminum nitride (AlN)-based film bulk acoustic resonators (FBARs) to construct filters are a promising approach to meet these requirements due to the high acoustic velocity of AlN, achievable large effective electromechanical coupling coefficient (K_{eff}^2) of FBAR and complementary metal oxide semiconductor compatibility [5,6]. B.P. Sorokin et al. have recently obtained an excitation of longitudinal bulk acoustic waves in a diamond-based high overtone bulk acoustic resonator at microwave and enhanced frequency bands up to 40 GHz [7,8]. However, with the rapid development of fifth-generation communication, the characteristics of AlN-based FBAR are further expected to be improved. For the design of the film bulk acoustic filters, K_{eff}^2 is a crucial parameter that affects the bandwidth and cutoff frequency of filters. In particular, doping method is an effective option to increase the electromechanical coupling coefficient (K_t^2) of piezoelectric material AlN, for example using Sc doping, thus obtaining an expected large bandwidth for AlN-based filters. Milena Moreira et al. have proved that using Sc doping with concentration of 15 at.% can achieve a two-times increase in the K_{eff}^2 , which is suitable for the applications needing broad bandwidth [9].

However, for specific requirements of bandwidth and frequency, we may need suitable K_{eff}^2 for FBARs in order to achieve the accurate control in passband of filters. Although different Sc doping concentrations in AlN can effectively obtain a different value of K_{eff}^2 for AlN-based FBARs, the Sc alloy targets for sputter technology are costly and it is difficult to produce arbitrary concentrations. AlN/AlScN bilayer composite film is a potential choice

to realize the modulation of K_{eff}^2 for FBARs, since we can modify the effective piezoelectric constants of the composite film using varying thickness ratios of AlN to AlScN films. In our previous work, AlN/AlScN bilayer composite film was selected to acquire a comparatively higher K_{eff}^2 of 7.8% for the Lamé Mode resonator [10]. Li et al. have a detailed investigation about the effective properties of AlN/AlScN bilayer composite film based on the Reuss model and Eshelby–Mori–Tanaka micromechanics theory and built an explicit relationship between piezoelectric constant d_{33} and the thickness ratio of AlN to AlScN [11]. Su et al., also found that AlN as a seed layer can effectively enhance the crystal quality and (002) orientation of AlScN film, which can be adopted to further improve the properties of FBAR and filter devices [12].

In this paper, we demonstrate the modulation of K_{eff}^2 for FBARs using different piezoelectric materials and propose the filter designs for specific bandpass based on the AlN/AlScN bilayer composite film. We investigate the influence of different thickness ratios of AlN to AlScN layer on the resonant characteristics and K_{eff}^2 of FBARs via finite element simulation. FBARs based on pure AlN, AlN/Al_{0.9}Sc_{0.1}N, and AlN/Al_{0.8}Sc_{0.2}N bilayer composite film are fabricated and we can obtain varying K_{eff}^2 for FBARs consistent with the simulated results. AlScN can effectively compensate the deficiency of AlN film in electromechanical coupling in the form of AlN/AlScN composite film. With a decreased thickness ratio of AlN to AlScN, an obvious increased K_{eff}^2 for FBARs can be realized. It is also verified that with AlN/Al_{0.8}Sc_{0.2}N composite film the filter for N77 sub-band (3.4 GHz–3.6 GHz) can be easily demonstrated, proving the feasibility using composite film to achieve the expected K_{eff}^2 for filter design.

2. Materials and Methods

In our work, the resonant characteristics of FBARs based on AlN and AlN/AlScN bilayer composite film were simulated using finite element method. All the piezoelectric materials were deposited by a magnet sputter (SPTS, Sigma fxP system, Newport, UK) under 200 °C. Pure Al metal, Al-Sc alloys with the atomic mass percent of Sc of 10% and 20%, respectively, were adopted when depositing the piezoelectric films [13]. Sputter power of 6 kW and bias power of 160 W were used for the film deposition with the flow rates of N₂ and Ar of 60 sccm and 20 sccm, respectively. X-ray diffraction (XRD) measurement (Rigaku, SmartLab SE with a Cu K α radiation, Tokyo, Japan) was used to characterize the crystal structure of piezoelectric films [13].

FBAR devices based on the micro-electromechanical systems process were fabricated on 725 μm -thick silicon substrates and the impedance curves of FBAR devices were measured using Keysight network analyzer (Keysight, N5222B, Santa Rosa, CA, USA) connecting to a Cascade Microtech's GSG probe station (FormFactor, Beaverton, OR, USA) [10]. The fabrication process flow is shown in Figure 1 [14]. The fabrication process started with etching Si to form the cavity (Figure 1a). The SiO₂ was deposited by physical vapor deposition as the sacrificial layer and chemical mechanical polishing was used to polish the surface of SiO₂ layer (Figure 1b) for the deposition of subsequent films. Then, AlN seed layer with a thickness of 25 nm and bottom Mo electrode layer were deposited using magnetron sputtering as shown in Figure 1c. Next, the piezoelectric layer (AlN, AlN/Al_{0.9}Sc_{0.1}N and AlN/Al_{0.8}Sc_{0.2}N composite films) was deposited by the magnet sputter and etched by inductively coupled plasma to open the bottom electrode pad as shown in Figure 1d. Another Mo layer was deposited and patterned as the top electrode layer (Figure 1e). Subsequently, the Au layer was deposited by electron beam evaporation and patterned (Figure 1f). The release windows were opened to release SiO₂ in the cavity (Figure 1g). Finally, the SiO₂ layer was wet-etched by HF/NH₃F mixed solution to empty the cavity and the resonators were fabricated completely (Figure 1h).

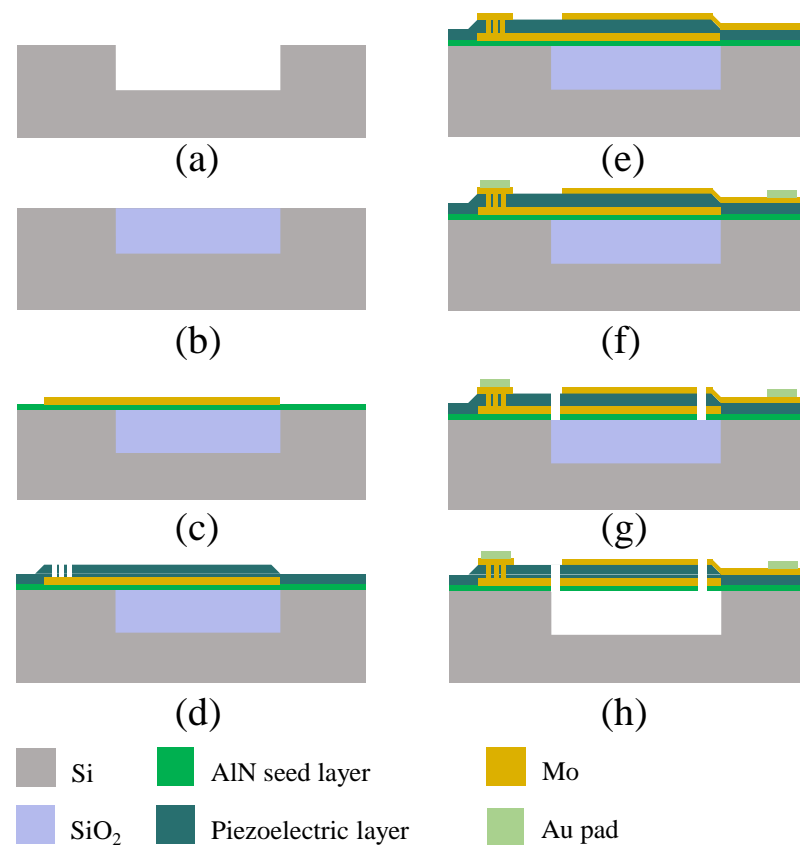


Figure 1. Main fabrication process steps of FBAR devices. (a) Etching Si substrate to form the cavity. (b) SiO₂ sacrificial layer deposition and polished. (c) AlN seed layer and bottom Mo electrode deposition. (d) Piezoelectric layer deposition and etched. (e) Top Mo electrode deposition and patterned. (f) Au pad layer deposition. (g) Release windows opened. (h) Releasing SiO₂ sacrificial layer to form the cavity.

3. Results and Discussions

Figure 2a,b show the schematic structures of a typical FBAR, which consists of a piezoelectric layer sandwiched between the top and bottom electrodes. The voltage or the electrical field between the two electrodes excites the acoustic wave. An air cavity is created between the bottom electrode and the substrate to trap the acoustic wave between the electrodes, as shown in Figure 2b. Figure 2c shows the working principle of a ladder filter based on FBAR, the inset in Figure 2c is the circuit topology of the ladder filters. The resonator has two resonant frequencies, one is the series resonant frequency f_s , at which the impedance Z_{min} can be very low, and the second one is a parallel resonant or anti-resonant frequency f_p , at which the impedance Z_{max} can be very high. The parallel resonator in the filter is tuned to be a slightly lower frequency by adding a mass loading layer on the top electrode. When f_{p2} representing the anti-resonant frequency of parallel resonators is chosen to be equal to or slightly lower than f_{s1} representing the series resonant frequency of series resonators, a passband is formed between the frequencies near f_{s2} and f_{p1} . The bandwidth of the filter is mainly determined by the effective coupling coefficient K_{eff}^2 of FBARs, which can be calculated by Equation (1). Therefore, for the filter design with a specific requirement in the passband, we need to consider the resonant frequencies of FBAR and seek a suitable K_{eff}^2 carefully [15–17].

$$K_{eff}^2 = \frac{\pi^2}{4} \frac{f_s}{f_p} \frac{f_p - f_s}{f_p} \quad (1)$$

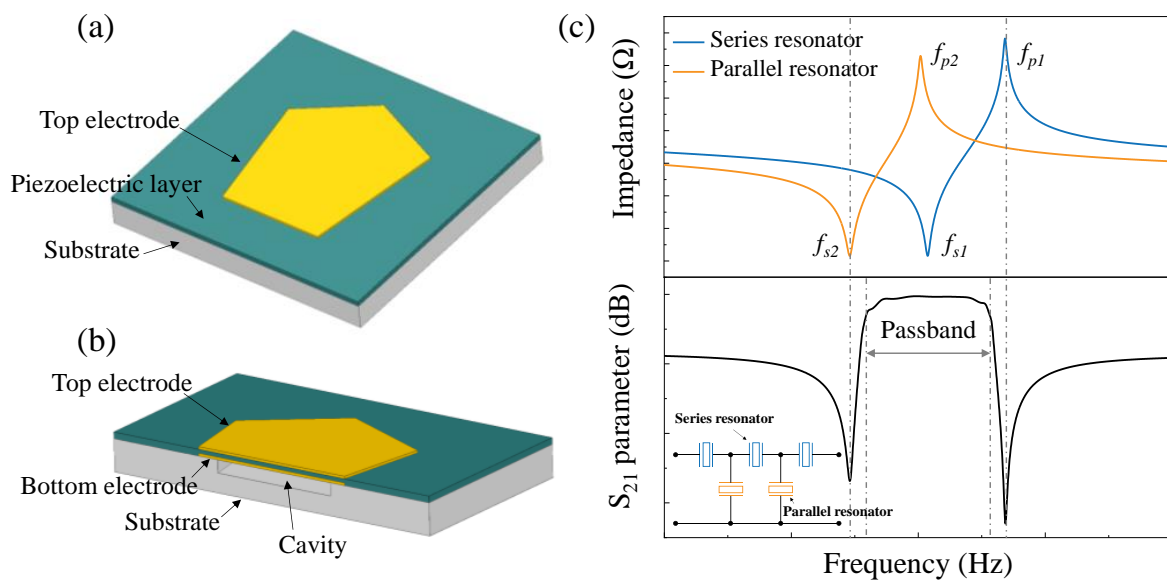


Figure 2. Structures of FBAR and characteristics of filters. (a) Schematic drawing of a typical FBAR. (b) The cross-sectional view of FBAR. (c) Working principle of filter based on FBARs. Inset shows the ladder circuit topology of filters.

For investigating the resonant characteristics of FBAR based on AlN/AlScN bilayer composite film with different thickness ratios, we used the finite element model to simulate the performances. Table 1 lists the material constants of AlN, Al_{0.9}Sc_{0.1}N, and Al_{0.8}Sc_{0.2}N piezoelectric films used for the simulation [11,18–21]. As shown in Figure 3, we obtained the impedance curves of FBARs with the pure AlN, AlN/Al_{0.9}Sc_{0.1}N, and AlN/Al_{0.8}Sc_{0.2}N composite films, respectively. The total thickness for piezoelectric layers is 1 μm, the thickness for both top and bottom Mo electrode is 200 nm. For FBAR based on 1 μm-thick AlN film, f_s is 2.65 GHz and f_p is 2.72 GHz. As shown in Figures 3a and 3b, for FBAR with AlN/AlScN composite films, with the increased thickness ratio of AlScN to AlN, the resonant frequency decreases, which can be contributed to the lower longitudinal acoustic velocity of AlScN compared with the acoustic velocity of AlN [4,22,23]. Figure 3c shows K_{eff}^2 of FBARs with different piezoelectric materials calculated by Equation (1). When using AlN/AlScN composite film to replace pure AlN film, we can obtain an increased K_{eff}^2 , and K_{eff}^2 for FBAR based on 1 μm-thick Al_{0.8}Sc_{0.2}N film can be twice of that when FBAR based on 1 μm-thick AlN film. It is also clear that using AlN/AlScN composite film with different thickness ratio can achieve an effective adjustment in K_{eff}^2 , which can be adopted when designing filters with the expected requirement in passband [24,25].

Table 1. Material constants of piezoelectric film used in the simulations.

	AlN	Al _{0.9} Sc _{0.1} N	Al _{0.8} Sc _{0.2} N
ρ (kg/m ³)	3260	3460	3560
ϵ_r	9.5	10.8	13.4
e_{31} (C/m ²)	−0.58	−0.62	−0.71
e_{33} (C/m ²)	1.55	1.67	2.08
e_{24} (C/m ²)	−0.48	−0.30	−0.27
C_{11} (GPa)	345	320	292
C_{12} (GPa)	125	127	130
C_{13} (GPa)	120	126	134
C_{33} (GPa)	395	324	258
C_{44} (GPa)	118	108	104
C_{66} (GPa)	110	110	91

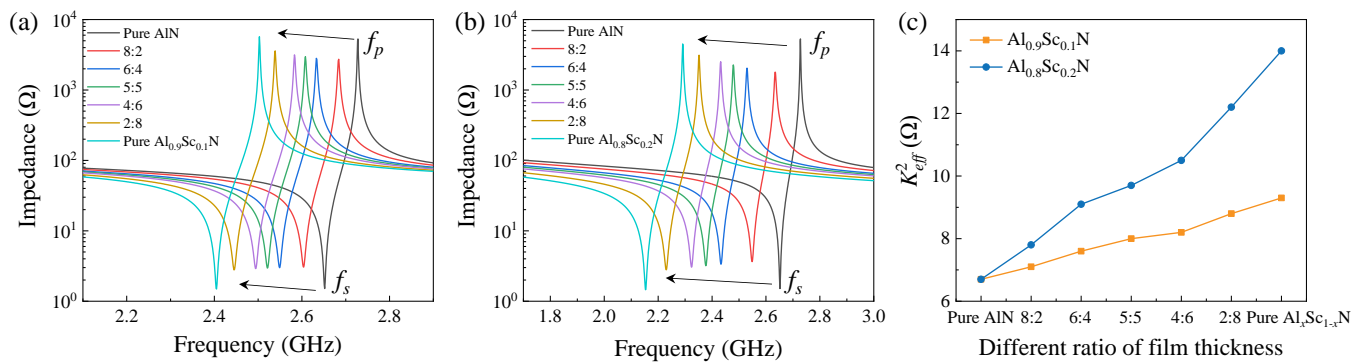


Figure 3. Simulated results of FBAR with different piezoelectric materials. (a) Simulated impedance curves of FBARs based on AlN/Al_{0.9}Sc_{0.1}N composite film with different thickness ratios. (b) Simulated impedance curves of FBARs based on AlN/Al_{0.8}Sc_{0.2}N composite film with different thickness ratios. (c) Calculated K_{eff}^2 of different FBARs.

We also deposited the piezoelectric films and fabricated FBARs to verify the simulated results. The pure AlN, Al_{0.9}Sc_{0.1}N, and Al_{0.8}Sc_{0.2}N with a thickness of 1 μm, respectively, were deposited on Si (100) substrate first. Further characterizations of piezoelectric materials were carried out using XRD as shown in Figure 4a; it is used to assess the (002) preferred orientation and crystal quality of piezoelectric films. Significant reflection peaks at around 35° to 36.0° associated with the (002) hexagonal AlN and AlScN films in patterns indicate that the piezoelectric films are well-crystallized with the *c* axis. The peak positions of Al_{0.9}Sc_{0.1}N and Al_{0.8}Sc_{0.2}N films shift due to the Sc doping [13,26,27]. The results of XRD rocking curves in the insets of Figure 4a show full width at half maximum (FWHM) of 1.49°, 1.62°, and 1.65° for 1 μm-thick AlN, Al_{0.9}Sc_{0.1}N, and Al_{0.8}Sc_{0.2}N films, respectively, suggesting a preferred *c*-axis crystal orientation as well [10,13]. Figure 4b shows the morphology of 1 μm-thick Al_{0.8}Sc_{0.2}N film caught by Scanning Electron Microscopy (SEM, Tescan, MIRA3, Brno, The Czech republic). Although small grain growth precipitates can be observed in the relative smooth surface of Al_{0.8}Sc_{0.2}N film, distinct clusters of particles, normally deteriorating the film quality, are absent [28,29].

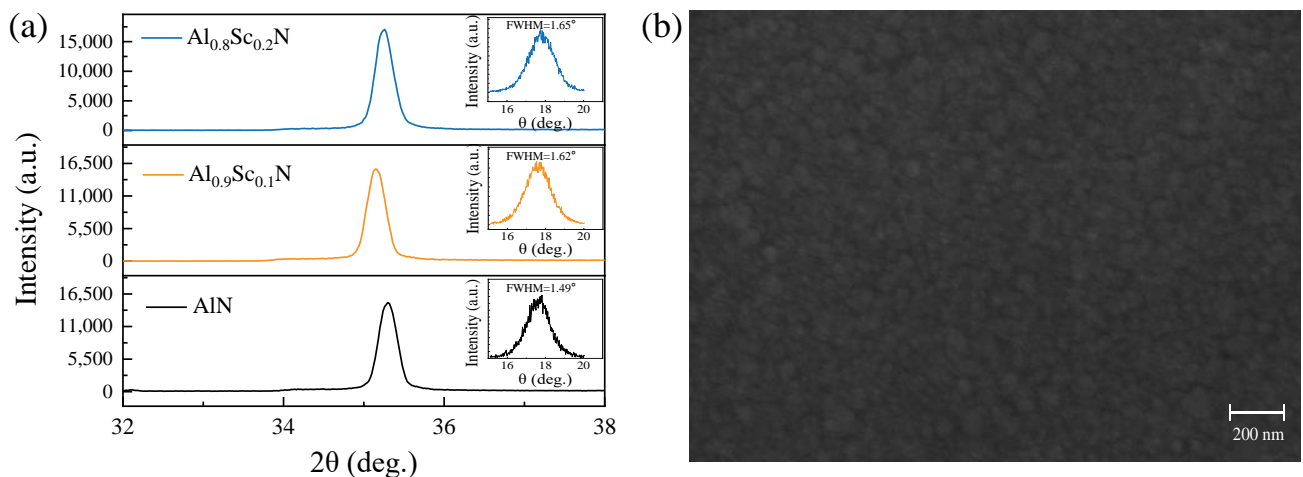


Figure 4. XRD results and morphology of piezoelectric materials. (a) XRD results of 1 μm-thick AlN, Al_{0.9}Sc_{0.1}N, and Al_{0.8}Sc_{0.2}N films, respectively. (b) Morphology of 1 μm-thick Al_{0.8}Sc_{0.2}N film.

In our work, for the fabricated FBARs, three different piezoelectric layers were deposited, including 1 μm-thick pure AlN, 1 μm-thick composite piezoelectric layer comprising 500 nm-thick AlN and 500 nm-thick Al_{0.9}Sc_{0.1}N, and 1 μm-thick composite piezoelectric layer comprising 500 nm-thick AlN and 500 nm-thick Al_{0.8}Sc_{0.2}N. Figure 5a shows the cross-sectional view of FBAR based on 1 μm-thick AlN/Al_{0.9}Sc_{0.1}N composite film, in

which the deposited thicknesses of AlN and Al_{0.9}Sc_{0.1}N layers are almost 500 nm, respectively, meaning we can achieve a delicate control for the film deposition. It can be seen that the films without obvious defects exhibit good flatness and crystal quality, which is essential for the performance of the device [27]. The vertical view of fabricated FBAR is shown in Figure 5b. It clearly shows that the resonant region is connected with signal pads via Mo anchors. The signal terminals on both sides of the resonator mean the input and output of electrical signals. Four release holes arranged at the corners of the edge are intended to etch the sacrificial layer fully and fabricate a resonant cavity.

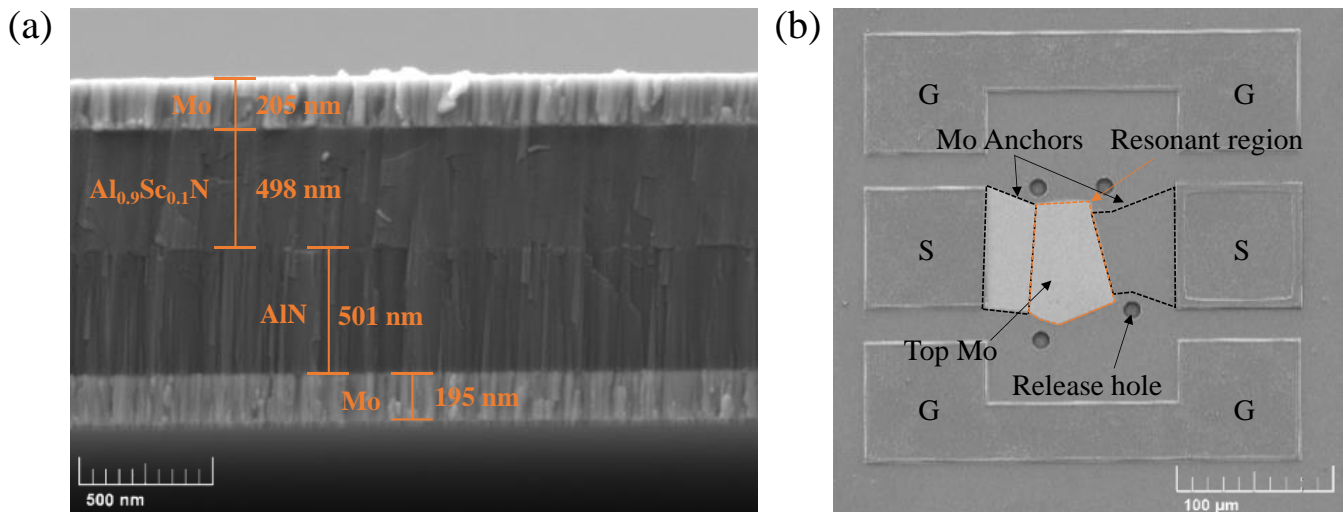


Figure 5. Characterization of piezoelectric film and FBAR device. (a) Cross-sectional view of AlN/Al_{0.9}Sc_{0.1}N composite film consisting of 500 nm-thick AlN and 500 nm-thick Al_{0.8}Sc_{0.2}N. (b) Vertical view of fabricated FBAR based on the AlN/Al_{0.9}Sc_{0.1}N composite film consisting of 500 nm-thick AlN and 500 nm-thick Al_{0.8}Sc_{0.2}N. The signal and ground pads are marked with “G” and “S” labels, respectively.

Figure 6 shows the tested impedance curves of FBARs based on pure AlN, AlN/Al_{0.9}Sc_{0.1}N, and AlN/Al_{0.8}Sc_{0.2}N composite film, respectively. The measured resonant frequencies and calculated K_{eff}^2 are closed with the simulated ones shown in Figure 3, which means that the estimated parameters in FBARs, including material constants, the thickness of each layer, are under control. Therefore, we can use the simulated conditions and results to evaluate the filter design. In order to verify the feasibility of composite films for filter design with specific bandwidth, we take the design of N77 sub band (3.4 GHz to 3.6 GHz) for example. Here, we adopt three piezoelectric films, including pure AlN film, AlN/Al_{0.8}Sc_{0.2}N composite film, and pure Al_{0.8}Sc_{0.2}N film, to design the filter. Figure 7a shows the schematic circuit of the designed filters. It consists of eight elements, including four series and four parallel resonators. Table 2 summarizes the thickness information of these three filters. The simulated results of the filters are plotted in Figure 7b. We can find that filter 1 with pure AlN film cannot meet the demand of 200 MHz bandwidth due to the limited intrinsic electromechanical coupling factor. As for filter 3 with pure Al_{0.8}Sc_{0.2}N film, it demonstrates a bandwidth larger than 200 MHz. Remarkably, by combining the characteristics of AlN and Al_{0.8}Sc_{0.2}N films, the proposed filter 2 can well meet the bandwidth requirement of 200 MHz demonstrating the serviceability using AlN/AlScN composite film with different thickness ratios for specific passband and frequency.

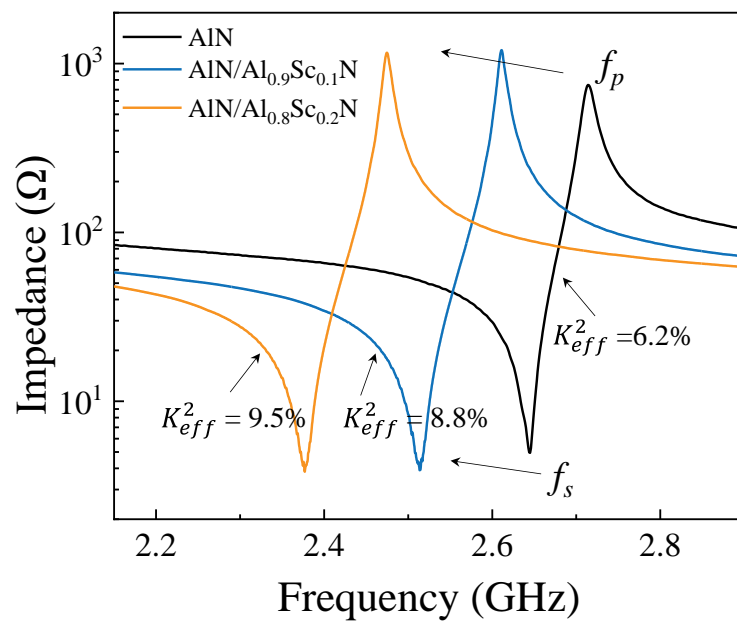


Figure 6. Tested impedance curves of FBARs with different piezoelectric materials: 1 μm -thick pure AIN, 1 μm -thick AIN/ $\text{Al}_{0.9}\text{Sc}_{0.1}\text{N}$ composite piezoelectric layer comprising 500 nm-thick AIN and 500 nm-thick $\text{Al}_{0.9}\text{Sc}_{0.1}\text{N}$, and 1 μm -thick AIN/ $\text{Al}_{0.8}\text{Sc}_{0.2}\text{N}$ composite piezoelectric layer comprising 500 nm-thick AIN and 500 nm-thick $\text{Al}_{0.8}\text{Sc}_{0.2}\text{N}$.

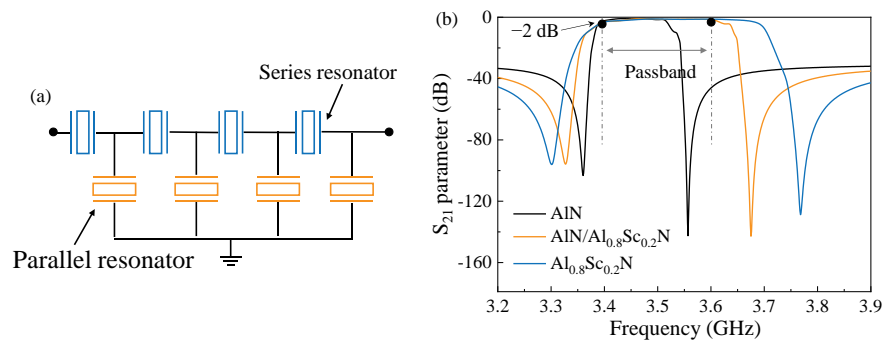


Figure 7. The proposed filter designs. (a) Schematic ladder circuit of the filter. (b) The comparison of simulated transmission responses among the filter 1 with AIN film, filter 2 with AIN/ $\text{Al}_{0.8}\text{Sc}_{0.2}\text{N}$ film, and filter 3 with $\text{Al}_{0.8}\text{Sc}_{0.2}\text{N}$ film, respectively.

Table 2. Structure parameters of the designed filters.

Dimension	Filter 1	Filter 2	Filter 3
Thickness of bottom Mo(nm)	184	103	102
Thickness of AIN (nm)	686	-	316
Thickness of $\text{Al}_{0.8}\text{Sc}_{0.2}\text{N}$ (nm)	-	679	473
Thickness of top Mo (nm)	164	103	100
Thickness of Mass loading Mo (nm)	21	41	30

4. Conclusions

In this work, we investigate the resonant characteristics of FBARs with different piezoelectric materials, including pure AIN, AlScN, and AIN/AlScN composite films, and explore the potential of using varying AIN/AlScN composite film to meet the requirements of filters with the expected bandwidth. We use finite element method to simulate the influence of different thickness ratio of AIN/AlScN composite film on the key parameter, K_{eff}^2 , and have a detailed insight in the resonant characteristics by fabricating FBARs based

on AlN, AlN/Al_{0.9}Sc_{0.1}N, and AlN/Al_{0.8}Sc_{0.2}N films. The results show that K_{eff}^2 can be increased by two times for FBAR based on 1 μm -thick Al_{0.8}Sc_{0.2}N film compared with that of FBAR based on 1 μm -thick pure AlN film. Adopting AlN/AlScN composite film with the adjustment in thickness ratio, we can achieve the delicate control on K_{eff}^2 , which can be an effective method for the further filter design. This work paves a way for filter demonstration using AlN/AlScN composite film with varying K_{eff}^2 to achieve the specific passband and frequency.

Author Contributions: Conceptualization, Y.C. and C.S.; Methodology, L.N.; Validation, Y.Z. (Yang Zou) and C.G.; Formal Analysis, Y.Z. (Yu Zhou) and Y.F.; Investigation, W.L. and Y.L.; Resources, J.B.S.; Writing, J.W. All authors have read and agreed to the published version of the manuscript.

Funding: This work was supported by the National Key R&D Program of China (Grant No. 2020YFB2008803), the fundamental research funds for the central universities under Grant No. 2042022kf1027.

Data Availability Statement: Data and code are available from the corresponding authors upon reasonable request.

Acknowledgments: We thank the Core Facility of Wuhan University for access to analytical equipment (XRD), the School of Power and Mechanical Engineering, Wuhan University, for access to analytical equipment (SEM, MIRA3).

Conflicts of Interest: The authors declare no conflict of interest.

References

1. Yim, M.; Jeon, B.; Yoon, G. Feasibility Study of Small-sized FBAR-based Bandpass Filter Covering Digital Dividend Band for LTE Services. *J. Semicond. Technol. Sci.* **2020**, *20*, 479–484. [[CrossRef](#)]
2. Wu, H.; Wu, Y.; Lai, Z.; Wang, W.; Yang, Q. A hybrid film-bulk-acoustic-resonator/coupled-line/transmission-line high selectivity wideband bandpass FBAR filter. *IEEE Trans. Microw. Theory Tech.* **2020**, *68*, 3389–3396. [[CrossRef](#)]
3. Bhadauria, A.; Panchal, B.; Varghese, S. RF bandpass filters using FBAR with fractal electrodes. In Proceedings of the 2018 IEEE MTT-S International Microwave and RF Conference (IMaRC), Kolkata, India, 28–30 November 2018; pp. 1–3.
4. Liu, Y.; Cai, Y.; Zhang, Y.; Tovstopyat, A.; Liu, S.; Sun, C. Materials, design, and characteristics of bulk acoustic wave resonator: A review. *Micromachines* **2020**, *11*, 630. [[CrossRef](#)] [[PubMed](#)]
5. Yi, X.; Zhao, L.; Ouyang, P.; Liu, H.; Zhang, T.; Li, G. High-Quality Film Bulk Acoustic Resonators Fabricated on AlN Films Grown by a New Two-Step Method. *IEEE Electron. Device Lett.* **2022**, *43*, 942–945. [[CrossRef](#)]
6. Wang, J.; Zheng, Y.; Ansari, A. Ferroelectric Aluminum Scandium Nitride Thin Film Bulk Acoustic Resonators with Polarization-Dependent Operating States. *Physica Status Solidi (RRL)—Rapid Res. Lett.* **2021**, *15*, 2100034. [[CrossRef](#)]
7. Sorokin, B.P.; Asafiev, N.O.; Kvashnin, G.M.; Scherbakov, D.A.; Terentiev, S.A.; Blank, V.D. Toward 40 GHz excitation of diamond-based HBAR. *Appl. Phys. Lett.* **2021**, *118*, 083501. [[CrossRef](#)]
8. Kvashnin, G.; Sorokin, B.; Asafiev, N.; Prokhorov, V.; Sotnikov, A. Peculiarities of the Acoustic Wave Propagation in Diamond-Based Multilayer Piezoelectric Structures as “Me1/(Al, Sc) N/Me2/(100) Diamond/Me3” and “Me1/AlN/Me2/(100) Diamond/Me3” under Metal Thin-Film Deposition. *Electronics* **2022**, *11*, 176. [[CrossRef](#)]
9. Moreira, M.; Bjurström, J.; Katardjev, I.; Yantchev, V. Aluminum scandium nitride thin-film bulk acoustic resonators for wide band applications. *Vacuum* **2011**, *86*, 23–26. [[CrossRef](#)]
10. Zhou, J.; Liu, Y.; Xu, Q.; Xie, Y.; Cai, Y.; Liu, J.; Liu, W.; Tovstopyat, A.; Sun, C. ScAlN/AlN Film-Based Lamé Mode Resonator With High Effective Electromechanical Coupling Coefficient. *J. Microelectromech. Syst.* **2021**, *30*, 677–679. [[CrossRef](#)]
11. Li, L.; Gu, X.; Gao, C.; Hu, S.; Wang, Y.; Zou, Y.; Liu, Y.; Liu, W.; Cai, Y.; Sun, C. Micromechanics predictions of effective elastic, piezoelectric and dielectric properties of composite piezoelectric films. *J. Microelectromech. Syst.* **2022**, *15*, 095503. [[CrossRef](#)]
12. Su, J.; Fichtner, S.; Ghori, M.Z.; Wolff, N.; Islam, M.; Lotnyk, A.; Kaden, D.; Niekietel, F.; Kienle, L.; Wagner, B. Growth of Highly c-Axis Oriented AlScN Films on Commercial Substrates. *Micromachines* **2022**, *13*, 783. [[CrossRef](#)]
13. Wang, Y.; Zou, Y.; Gao, C.; Gu, X.; Ma, Y.; Liu, Y.; Liu, W.; Soon, J.B.W.; Cai, Y.; Sun, C. Effects of Electric Bias on Different Sc-Doped AlN-Based Film Bulk Acoustic Resonators. *Electronics* **2022**, *11*, 2167. [[CrossRef](#)]
14. Chauhan, S.S.; Joglekar, M.M.; Manhas, S.K. Influence of process parameters and formation of highly c-axis oriented AlN thin films on mo by reactive sputtering. *J. Electron. Mater.* **2018**, *47*, 7520–7530. [[CrossRef](#)]
15. Gao, C.; Zou, Y.; Zhou, J.; Liu, Y.; Liu, W.; Cai, Y.; Sun, C. Influence of Etching Trench on K_{eff}^2 of Film Bulk Acoustic Resonator. *Micromachines* **2022**, *13*, 102. [[CrossRef](#)] [[PubMed](#)]
16. Ding, R.; Xuan, W.; Dong, S.; Zhang, B.; Gao, F.; Liu, G.; Zhang, Z.; Jin, H.; Luo, J. The 3.4 GHz BAW RF Filter Based on Single Crystal AlN Resonator for 5G Application. *Nanomaterials* **2022**, *12*, 3082. [[CrossRef](#)]

17. Nam, K.; Park, Y.; Ha, B.; Shim, D.; Song, I.; Pak, J.; Par, G.J. Piezoelectric properties of aluminum nitride for thin film bulk acoustic wave resonator. *J. Korean Phys. Soc.* **2005**, *47*, 309.
18. Ambacher, O.; Christian, B.; Feil, N.; Urban, D.; Elsässer, C.; Prescher, M.; Kirste, L.J. Wurtzite ScAlN, InAlN, and GaAlN crystals, a comparison of structural, elastic, dielectric, and piezoelectric properties. *J. Appl. Phys.* **2021**, *130*, 045102. [[CrossRef](#)]
19. Zhang, S.; Fu, W.Y.; Holec, D.; Humphreys, C.; Moram, M. Elastic constants and critical thicknesses of ScGaN and ScAlN. *J. Appl. Phys.* **2013**, *114*, 243516. [[CrossRef](#)]
20. Caro, M.A.; Zhang, S.; Riekkinen, T.; Ylilammi, M.; Moram, M.A.; Lopez-Acevedo, O.; Molarius, J.; Laurila, T. Piezoelectric coefficients and spontaneous polarization of ScAlN. *J. Phys. Condens. Matter* **2015**, *27*, 245901. [[CrossRef](#)] [[PubMed](#)]
21. Wingqvist, G.; Tasnadi, F.; Zukauskaitė, A.; Birch, J.; Arwin, H.; Hultman, L. Increased electromechanical coupling in $w - \text{Sc}_x\text{Al}_{1-x}\text{N}$. *Appl. Phys. Lett.* **2010**, *97*, 112902. [[CrossRef](#)]
22. Wang, W.; Mayrhofer, P.M.; He, X.; Gillinger, M.; Ye, Z.; Wang, X.; Bittner, A.; Schmid, U.; Luo, J. High performance AlScN thin film based surface acoustic wave devices with large electromechanical coupling coefficient. *Appl. Phys. Lett.* **2014**, *105*, 133502. [[CrossRef](#)]
23. Kurz, N.; Ding, A.; Urban, D.F.; Lu, Y.; Kirste, L.; Feil, N.M.; Žukauskaitė, A.; Ambacher, O. Experimental determination of the electro-acoustic properties of thin film AlScN using surface acoustic wave resonators. *J. Appl. Phys.* **2019**, *126*, 075106. [[CrossRef](#)]
24. Wang, J.; Park, M.; Mertin, S.; Pensala, T.; Ayazi, F.; Ansari, A. A film bulk acoustic resonator based on ferroelectric aluminum scandium nitride films. *J. Microelectromech. Syst.* **2020**, *29*, 741–747. [[CrossRef](#)]
25. Yokoyama, T.; Iwazaki, Y.; Onda, Y.; Nishihara, T.; Sasajima, Y.; Ueda, M. Highly piezoelectric co-doped AlN thin films for wideband FBAR applications. *IEEE Trans. Ultrason. Ferroelectr. Freq. Control.* **2015**, *62*, 1007–1015. [[CrossRef](#)] [[PubMed](#)]
26. Tang, J.; Niu, D.; Yang, Y.; Zhou, D.; Yang, C. Preparation of ScAlN films as a function of sputtering atmosphere. *J. Mater. Sci. Mater. Electron.* **2016**, *27*, 4788–4793. [[CrossRef](#)]
27. Dargis, R.; Clark, A.; Ansari, A.; Hao, Z.; Park, M.; Kim, D.; Yanka, R.; Hammond, R.; Debnath, M.; Pelzel, R. Single-Crystal Multilayer Nitride, Metal, and Oxide Structures on Engineered Silicon for New-Generation Radio Frequency Filter Applications. *Phys. Phys. Phys. Status Solidi A* **2020**, *217*, 1900813. [[CrossRef](#)]
28. Fichtner, S.; Reimer, T.; Chemnitz, S.; Lofink, F.; Wagner, B. Stress controlled pulsed direct current co-sputtered $\text{Al}_{1-x}\text{Sc}_x\text{N}$ as piezoelectric phase for micromechanical sensor applications. *APL Mater.* **2015**, *3*, 116102. [[CrossRef](#)]
29. Sandu, C.S.; Parsapour, F.; Mertin, S.; Pashchenko, V.; Matloub, R.; LaGrange, T.; Heinz, B.; Murali, P. Abnormal grain growth in AlScN thin films induced by complexion formation at crystallite interfaces. *Phys. Status Solidi A* **2019**, *216*, 1800569. [[CrossRef](#)]